

Triclinic BiFeO₃: A new magnetic phase with enhanced magnetism and resistivity

Md Sariful Sheikh ^{a, 1, †, *}, Tushar K. Bhowmik ^{a, †, *}, Alo Dutta ^b, Sujoy Saha ^c, Chhatra R. Joshi ^d, T. P. Sinha ^a

^a Department of Physics, Bose Institute, 93/1, A.P. C. Road, Kolkata-700009, India

^b Department of Condensed Matter Physics and Material Sciences, S.N. Bose National Centre for Basic Sciences, Block-JD, Sector-III, Salt Lake, Kolkata, 700106, India

^c Department of Materials Engineering, Indian Institute of Science, Bangalore 560012, India

^d Department of Physics and Astronomy, The University of Alabama, Tuscaloosa, AL 35487, USA

Abstract:

The magnetic and transport properties of BiFeO₃/La₂NiMnO₆ (BFO/LNMO) composite have been investigated both experimentally and theoretically. Unlike the normal rhombohedral (R3c) phase, BFO in the composites is crystallized in the triclinic phase (P1). Interestingly, the composites demonstrate a significant enhancement in the magnetization, magnetoelectric coupling and show higher resistivity than that of the regular BFO (R3c). As LNMO has its Curie temperature at 280 K, the room temperature and above room temperature magnetic contribution in the composites is expected to be from the triclinic BFO phase. Experimentally observed enhancement in magnetization is validated using classical Monte Carlo simulation and density functional theory (DFT) calculations. The calculated band structures show a more delocalized band edge in triclinic BFO which suggests the higher carrier effective mass i.e., enhanced resistivity in triclinic BFO as compared to the rhombohedral BFO. Overall, this study reveals triclinic BFO as the promising room temperature multiferroic phase which is helpful to optimize the multiferroicity of BFO and achieve wider applications in future.

¹ Present address: Department of Materials Science and Engineering, University of Wisconsin Madison, 1509 University Ave, Madison, WI 53706, United States

[†] Authors contributed equally to this work.

Introduction:

ABO₃ type multiferroic perovskite oxide BiFeO₃ has attracted a great research attention owing to the rare coexistence of ferroelectric and anti-ferromagnetic ordering with high transition temperatures (Curie temperature, $T_c \sim 1100$ K and Neel temperature, $T_N \sim 640$ K) [1-3]. Since the initial demonstration of robust coupling between these two order parameters, the promising possibility of various fascinating applications in data storage systems, spintronics, microelectronics, and sensors has been explored [4-7]. BiFeO₃ shows highly distorted rhombohedral (R3c) perovskite structure at room temperature and G-type antiferromagnetic ordering, which originates from the super exchange interactions between the neighbouring half-filled d-orbital of Fe³⁺ cation and occupied 2p-orbital of O²⁻ anion [8]. Recently, exploiting these properties, low energy consuming non-volatile magnetoelectric spin-orbit device has been proposed [9]. However, the high leakage current due to low resistivity, low saturation magnetization, low remnant magnetization and weak magnetoelectric coupling in BiFeO₃ are the issues to be addressed before its realistic applications in the next generation logic and memory devices [1, 10-12]. The interplay among the crystal structure, charge, spin, and orbital degrees of freedom provides a fertile research ground for improving the multiferroic properties in BFO [7, 13, 14]. Modifying the crystal structure, spin ordering, and band gap are keys to acquiring better electrical and magnetic properties. Various approaches including, the elemental substitution at the A and/or B sites, high quality crystal formation, reducing the particle size, hetero-structure and solid solution formation have been turned out to be very effective to improve the multiferroic properties of BFO [8, 15-16]. Although promising, the multiferroicity and magnetoelectric coupling in either single phase BFO or composites/heterostructure are required to be further improved for its practical implementation, which demand more fundamental understanding of its structure-property correlation and its exploitation.

In this work, an experimental investigation combined with the theoretical calculations using the density functional theory (DFT) and Monte Carlo simulation (MCS) have been performed on the magnetic and electric properties of the $(1-x)\text{BFO} + (x)\text{La}_2\text{NiMnO}_6$ (LNMO) ($x = 0.0, 0.1, 0.2$ and 0.3) composites. The double perovskite oxide LNMO is another widely studied below room temperature ferromagnetic semiconductor (Curie temperature, $T_C \sim 280$ K) with rich physical properties [17-18]. In our previous study we have observed that the large lattice parameters mismatch between BFO and LNMO lattice makes both the lattices highly strained and pushes the BFO lattice from being regular rhombohedral (R3c) to the lowest possible triclinic (P1) phase [19]. Previously, Chen et al observed the formation of ferroelectric triclinic phase in the mixed phase regions of highly strained BiFeO_3 thin film and predicted large piezoelectric response in it [20]. Though the synthesis of multiferroic BFO based composites/heterostructures is a very effective approach to improve its multiferroic properties, most of the studies are on the regular rhombohedral, and strain-mediated monoclinic, orthorhombic, and tetragonal BFO systems [21-23]. But, the magnetic and electric properties of the triclinic BFO are yet to be fully explored. To get the fundamental insight into the electronic properties, we have also performed the DFT calculation on the triclinic BFO and compared it with that of the rhombohedral BFO.

The combined experimental and theoretical study demonstrates that triclinic BFO structure (P1) has the promising potential to overcome the low magnetism, weak magnetodielectric coupling and high leakage current of rhombohedral BiFeO_3 . The modified structure of BFO (P1) possesses increased electrical resistivity, and an increased spin canting resulting in the significantly enhanced magnetisation as compared to the conventional R3c BFO.

Methodology:

The composites are synthesised using sol-gel method and a brief description of the synthesis procedure is represented in the supporting information file. The electrical measurements are performed using circular discs (8 mm diameter and ~ 1 mm thick) of the BFO/LNMO composites. The vibrating sample magnetometer (EverCool Quantum Design VSM magnetometer; Lakeshore) is used to study the magnetization of the as prepared pellets in the temperature range from 80 K to 400 K at zero field and an applied magnetic field of 5 kOe. The magnetic hysteresis properties are studied at 80 and 300 K. For the electrical measurements, the pellets were polished on both sides and silver electrodes were deposited using ultrapure silver paste (Ladd Research Industries. Inc). The capacitance (C) and conductance (G) were measured in the frequency range from 42 Hz to 1.6 MHz and in the temperature range 303 to 683 K using an LCR meter (3532-50, Hioki). The real part of the complex dielectric constant ($\epsilon' = C/C_o$, where $C_o = \epsilon_o A/t$, ϵ_o is the permittivity of free space, t is the pellet thickness, and A is the surface area), imaginary part ($\epsilon'' = Gx/\omega\epsilon_o$, ω is the angular frequency) of the complex dielectric constant, dielectric loss factor ($\tan \delta = \epsilon''/\epsilon'$) and Ac electrical conductivity ($\sigma = Gx$, $x = t/A$) were obtained from the frequency dependence of C and G .

Results and discussion:

The detailed structural characteristics are reported in our previous work [19], and a summary of the crystal structures and lattice parameters of the composite components are represented in Table S1 and Figure S1. The pure BiFeO₃ ($x = 0.0$) is crystallised in the usual rhombohedral (space group R3c; $a = b = c = 5.643 \text{ \AA}$, $\alpha = \beta = 90^\circ$, $\gamma = 120^\circ$) phase as shown in Figure 1(a). But in the BFO/LNMO composite BFO is crystallised in the triclinic (space group P1; $a = 3.931 \text{ \AA}$, $b = 3.936 \text{ \AA}$, $c = 3.956 \text{ \AA}$, $\alpha = 90.32^\circ$, $\beta = 90.24^\circ$, $\gamma = 89.98^\circ$) phase as shown in Figure 1(b), LNMO is crystallised in the monoclinic structure. Figure 1(c, d) show that the $\langle \text{Fe} - \text{O} - \text{Fe} \rangle$

bond angle and FeO₆ octahedra volume, which play a crucial role in the magnetic and electric properties of BFO, significantly reduces from rhombohedral to the triclinic BFO in the composites, are discussed later.

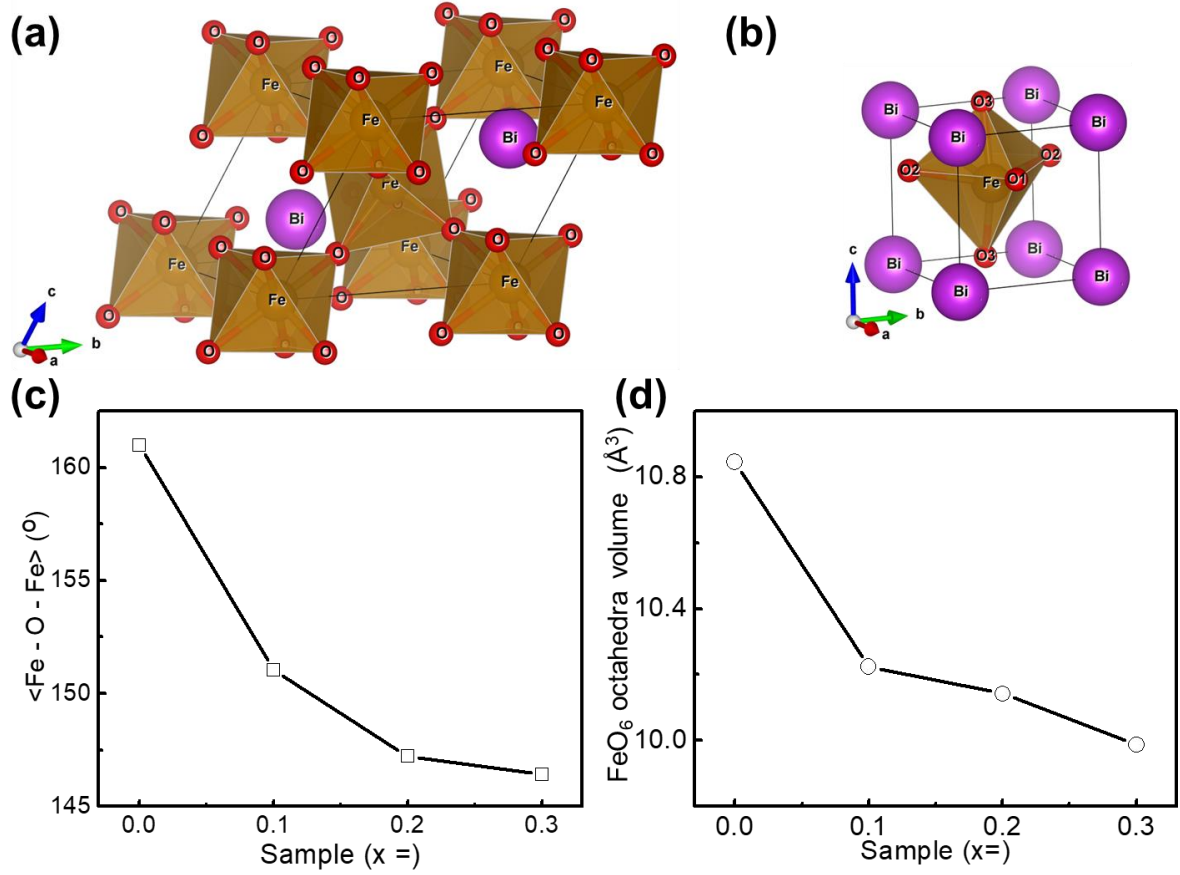


Figure 1: Unit cell representation of (a) Rhombohedral BFO and (b) triclinic BFO; LNMO loading dependence of (c) <Fe – O – Fe> bond angle, (d) FeO₆ octahedra volume.

Figure 2(a) shows the logarithmic angular frequency, $\log(\omega)$ dependence of the AC conductivity, $\sigma(\omega)$ which exhibits the typical semiconductor behaviour with a plateau region in the low frequency region. The conductivity value in the low frequency plateau is nearly equal to the DC conductivity value (σ_{dc}) and the conduction mechanism is also similar to its DC conduction mechanism i.e., short range translational hopping of the charge carriers from one localised site to another [24]. With the increase in frequency the probability of successful hopping decreases and the probability of the unsuccessful hopping i.e., localised back and forth

movement of the charge carriers increases. As the frequency exceeds the critical hopping frequency (ω_H), the ratio of the successful to unsuccessful hopping starts to decrease which results in a dispersive conductivity in the higher frequency region. The $\sigma(\omega)$ can be fitted and explained by the following Jonscher power law [25, 26],

$$\sigma(\omega) = \sigma_{dc} \left[1 + \left(\frac{\omega}{\omega_H} \right)^n \right]$$

where, n is a dimensionless parameter varying from 0 to 1. The fitted values of n for the samples x = 0.0, 0.1, 0.2 and 0.3 are 0.9, 0.91, 0.3 and 0.8, respectively, and the fitted values of ω_H are 2900, 5500, 12500 and 165000, respectively. The higher values of the ω_H in the composites suggest the less frequency dependence as compared to the rhombohedral BFO. The resistivity values ($1/\sigma_{dc}$) obtained from the σ_{dc} values are plotted in **Figure 2(b)**, which shows that with the LNMO loading the resistivity of the samples increases up to x = 0.2. This resistivity change may be attributed to the structural transformation from rhombohedral (R3c) BFO to triclinic (P1) BFO. The electronic structure and electrical properties in perovskites are determined by the hybridisation strength between Fe and O atoms in the FeO_6 octahedra. The reduced $\langle \text{Fe} - \text{O} - \text{Fe} \rangle$ bond angle decreases the hybridisation strength between Fe-3d and O-2p orbitals in triclinic BFO which is responsible for the increased resistivity in the composites. On the other hand, the excess loading of the relatively narrow band gap LNMO forms interconnected electrical networks which results in the reduced resistivity in x = 0.3.

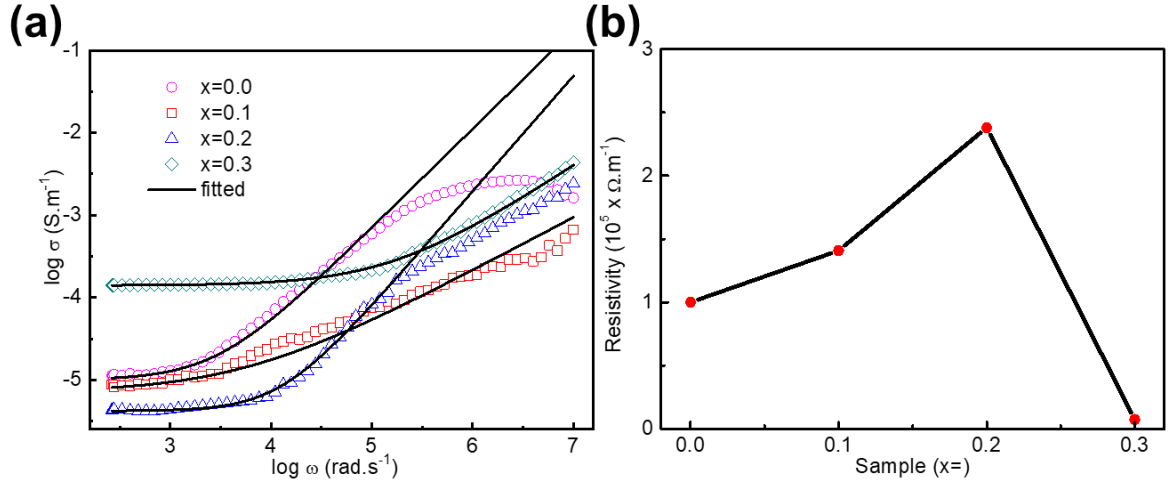


Figure 2: (a) Logarithmic angular frequency dependence of ac conductivity. Solid lines indicate the power law fitted data. (b) Room temperature dc-conductivity plot as a function of LNMO molar concentration.

The low temperature dependence of the magnetization plots (in the temperature range 80-400 K) (**Figure 3(a)**) of the samples at 5 kG shows a large increment in the magnetization in the composites as compared to the pure rhombohedral BFO. A sudden rise in the magnetisation at temperature ~ 280 K has been observed in the composites as the temperature decreases, which is related to the ferromagnetic transition of LNMO. In general, the LNMO lattice offers both the long-range ordering of Ni and Mn cations and forms the ordered monoclinic ($P2_1/n$) or rhombohedral ($R\bar{3}m$) structures; and disordered orthorhombic ($Pbnm$) phase [27-28]. Ordered LNMO phases have the $\text{Ni}^{2+}/\text{Mn}^{4+}$ oxidation states and the $\text{Ni}^{2+}\text{--O--Mn}^{4+}$ super exchange interaction generates ferromagnetism with the Curie temperature ($T_{\text{CM}} \sim 280$ K) just below the room temperature. Whereas disordered LNMO phase has trivalent $\text{Ni}^{3+}/\text{Mn}^{3+}$ oxidation states and the $\text{Ni}^{3+}\text{--O--Mn}^{3+}$ vibronic super exchange interaction incorporates ferromagnetism with a lower T_{CM} (~ 150 K) [29]. Hence, the Curie temperature ($T_{\text{C1}} \sim 280$ K, as shown in **Figure S2**) suggests the existence of ordered LNMO phase in the composites and the magnetic contribution above 280 K is completely attributed to the other

source of origin which is in this case triclinic BFO phase. The plots of the magnetisation (M) as a function of magnetic field (H) at temperatures 80 and 300 K are shown in **Figure 3(b) and Figure 3(c)**, respectively. Pure BFO presents the simple linear M(H) dependence with very small remanent magnetization (M_r) and saturation magnetization. The summary of the magnetic parameters at 300 and 80 K are tabulated in **Table S2 and S3**. It is noteworthy to mention here that a large increment in the magnetisation has been observed in the composites. The remanent magnetization for the samples with $x = 0.0, 0.1, 0.2$ and 0.3 are 0.0003, 0.304, 0.425, 0.332 emu/gm, respectively. The room temperature remanent magnetization in the samples with $x = 0.1, 0.2$ and 0.3 are almost increased by 1000, 1400 and 1100 times, respectively, as compared to the pure BFO. The room temperature magnetization at 14 kG for the samples $x = 0.0, 0.1, 0.2$ and 0.3 are 0.09, 0.92, 1.55, 1.50 emu/gm, respectively. The magnetization for the samples $x = 0.1, 0.2$ and 0.3 are increased by 10.2, 17.2 and 16.6 times, respectively. The comparison of the room temperature remanent magnetization of (0.8BFO + 0.2LNMO) with some other reported BFO based bulk samples as tabulated in **Table S4**, suggests that this triclinic BFO has much higher magnetization as compared to other phases of BFO. However, the lowering of BFO concentration may be the reason for decreasing magnetisation in the sample with $x = 0.3$. The MH loop at 803 K also shows similar behaviour suggesting increased magnetic moment of the composites (**Figure S3**). The temperature dependent magnetic moment plot (**Figure S4**) at high temperature region reveals anti-ferromagnetic behaviour in sample with $x = 0.1$ which is like regular rhombohedral BFO. Whereas the sample with $x = 0.3$ shows ferromagnetic behaviour suggesting AFM to FM transition in BFO. The overall increment in magnetisation in the composites may be because of the triclinic crystal structure of BFO. The magnetisation in multiferroic BFO depends on the antiferromagnetic sublattice angularity, with the Dzyaloshinski-Moriya interaction (DMI) playing the key role. The DM interaction leads to the spin canting resulting in the appearance

of a rather small total FM moment in an AFM structure, thus enhancing the magnetism. Here the decreased $\langle \text{Fe} - \text{O} - \text{Fe} \rangle$ bond angle in the triclinic BFO increases the canting of spins and, hence, improves the magnetization as compared to the R3c BFO [30-32].

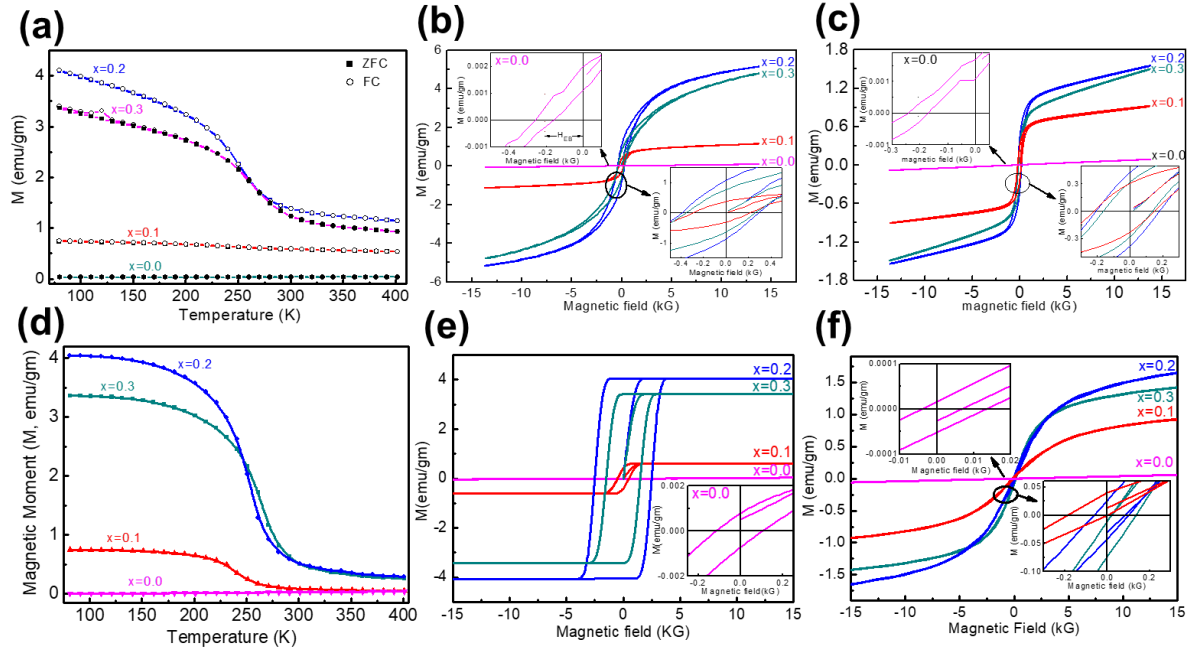


Figure 3: (a) Temperature dependent magnetisation plots in both zero-field cooling and field cooling condition (1 kG), Experimental MH loop at (b) 80 K and (c) 300 K. (d) Monte-Carlo simulation of magnetisation versus temperature. Monte-carlo simulated MH loop at (e) 80 K and (f) 300 K.

We have also performed the Monte Carlo simulations under the Metropolis algorithm to investigate the magnetic properties of the BFO/LNMO solid solutions and the detailed calculation formalism are described in the supporting information file. As shown in **Figure 3(d)**, the simulated temperature-dependent magnetization plots of the systems follow the same pattern as the experimental data. We have also investigated the effect of external magnetic fields on the room temperature hysteresis loops of the BFO/LNMO composite systems. **Figure 3(e)** shows that the M-H loops at 80 K manifest the FM nature of the composites compared to the AFM R3c BFO. Therefore, the FM nature of the composites may be attributed to the FM

nature of LNMO. However, the simulated MH loops above the Curie temperature of LNMO, i.e., at 300 K, as shown in **Figure 3(f)** suggest the anti-ferromagnetic nature of the solid solutions and a significant increment in the magnetization compared to pure BFO, which agree with the experimental data.

The appearance of a dielectric anomaly near the magnetic transition temperature is evidence of the multiferroic magnetoelectric coupling [33]. The temperature dependent dielectric constant plot of the rhombohedral BFO and the composite with $x=0.2$ as shown in Figure 4(a) demonstrates the magnetoelectric coupling in these materials. Interestingly, the composite with $x = 0.2$ shows significantly enhanced dielectric anomaly near the magnetic transition temperature at 650 K suggesting much stronger magnetoelectric coupling in it as compared to the R3c BFO. The dielectric loss tangent ($\tan\delta$) as shown in Figure 4(b) also demonstrates much lower dielectric loss in the composite with $x = 0.2$. Overall, these experimental studies reveal the significantly higher magnetization and magnetoelectric coupling in the triclinic BFO based composite, and motivate to further explore this triclinic BFO structure using density functional theory calculations formalism.

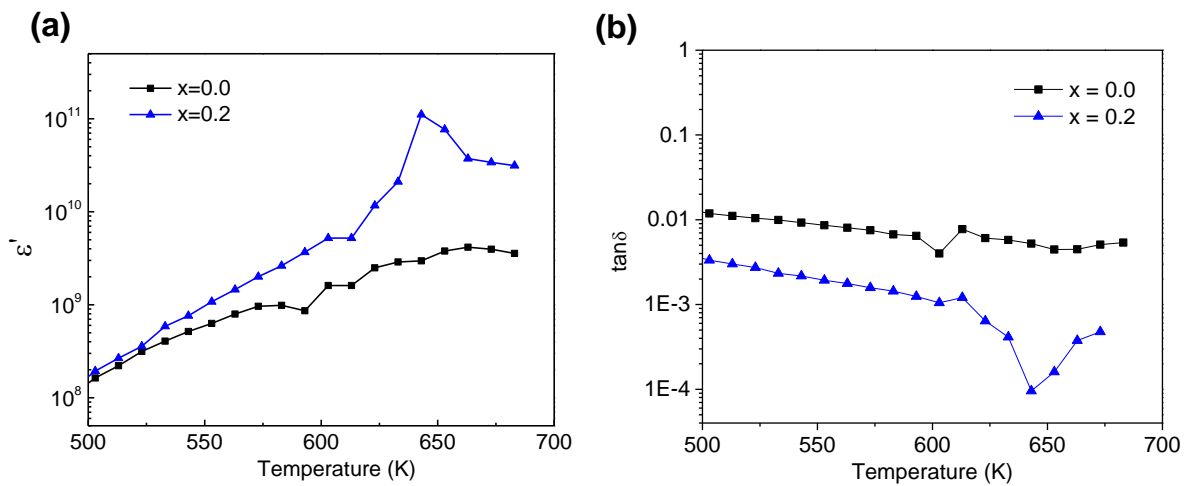


Figure 4: (a) Temperature dependence of the real part of the dielectric constant (ϵ'), and (d) dielectric loss factor at frequency 4.8 MHz.

The results obtained in the triclinic BFO-based composites motivate the DFT analysis of the triclinic and rhombohedral BFO. The spin polarised band structure of the rhombohedral BFO is shown in **Figure 5(a, b)**, and the band structure of triclinic BFO is presented in **Figure 5(c, d)**. The DFT calculated lowest band gap for the R3c BFO phase for the spin-up condition is 2 eV, consistent with the experimental band gap of rhombohedral BFO [19]. On the other hand, the triclinic phase shows an increased band gap of 2.2 eV, as observed in the spin-up condition. Furthermore, the rhombohedral VBM at the Γ , X, and K points and the conduction band minima (CBM) at the W and Δ symmetry points also show relatively more dispersion as compared to the VBM at the N and Γ points and the CBM at the N and Δ points of triclinic BFO, respectively. Interestingly, less dispersion at the CBM and VBM manifests the higher effective mass of the charge carriers, electron, and hole. Hence, due to the wider band gap and increased effective mass, the triclinic BFO is desired to possess higher resistivity than the rhombohedral BFO, which is consistent with the experimental DC conductivity study. This observed higher resistance helps to reduce the leakage current of BFO, which has been a main shortcoming of BFO for device use.

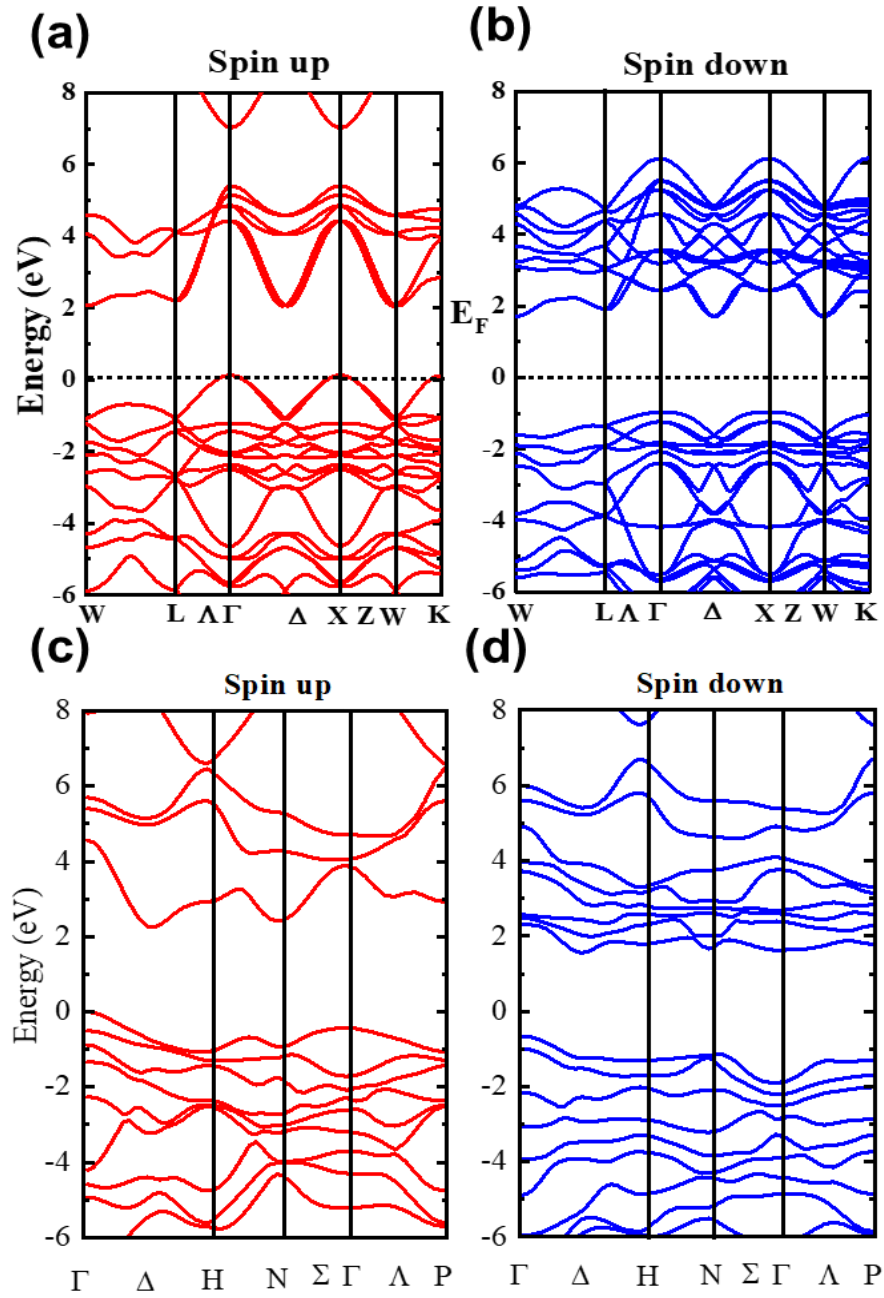


Figure 5: Band structure of rhombohedral BFO for (a) spin up and (b) spin down configuration. Band structure of triclinic BFO for (c) spin up and (d) spin down configuration.

The spin polarised density of states (DOS) of the R3c and P1 BFO are shown in **Figure 6 (a) and (b)** respectively. The partial DOS analysis shows that DOS in VBM and CBM is mainly dominated by the Fe-3d and O-2p states with slight contribution from the Bi-6p state in both R3c and P1 BFO. However, the overlap of O-2p and Fe-3d states is more prominent in

triclinic BFO than that in the rhombohedral BFO, suggesting the stronger covalent nature of Fe-O bonds in triclinic BFO. The calculated spin magnetic moments for the Bi, Fe and O atoms in rhombohedral BFO are $0.049 \mu_B$, $3.56 \mu_B$ and $0.33 \mu_B$, respectively. The value of the calculated magnetic moment of Fe^{3+} ion is consistent with previous experiment and theoretical results. The measured magnetic moment of Fe^{3+} ion using low-temperature neutron-diffraction in R3c BFO is $3.75 \mu_B$ [34]. The previous DFT study shows that the magnetic moment of Fe^{3+} ion in R3c BFO is $3.65 \mu_B$ [35]. The spin magnetic moments for the Bi, Fe and O atoms in triclinic P1 structure are $0.014 \mu_B$, $3.97 \mu_B$ and $0.19 \mu_B$, respectively, which manifest the increased magnetic moment in triclinic BFO structure. The theoretical value of the spin only magnetic moment of Fe^{3+} ion is $5.91 \mu_B$, which is calculated from $\sqrt{n(n+2)}$, (n = number of unpair electrons). So, the calculated magnetic moment from DFT is less than the theoretical one. The hybridization between Fe-3d and O-2p orbitals is responsible for this [36]. **Figure 6 (c) and (d)** represent the magnetic spin structure of BFO, determined from the DFT calculations.

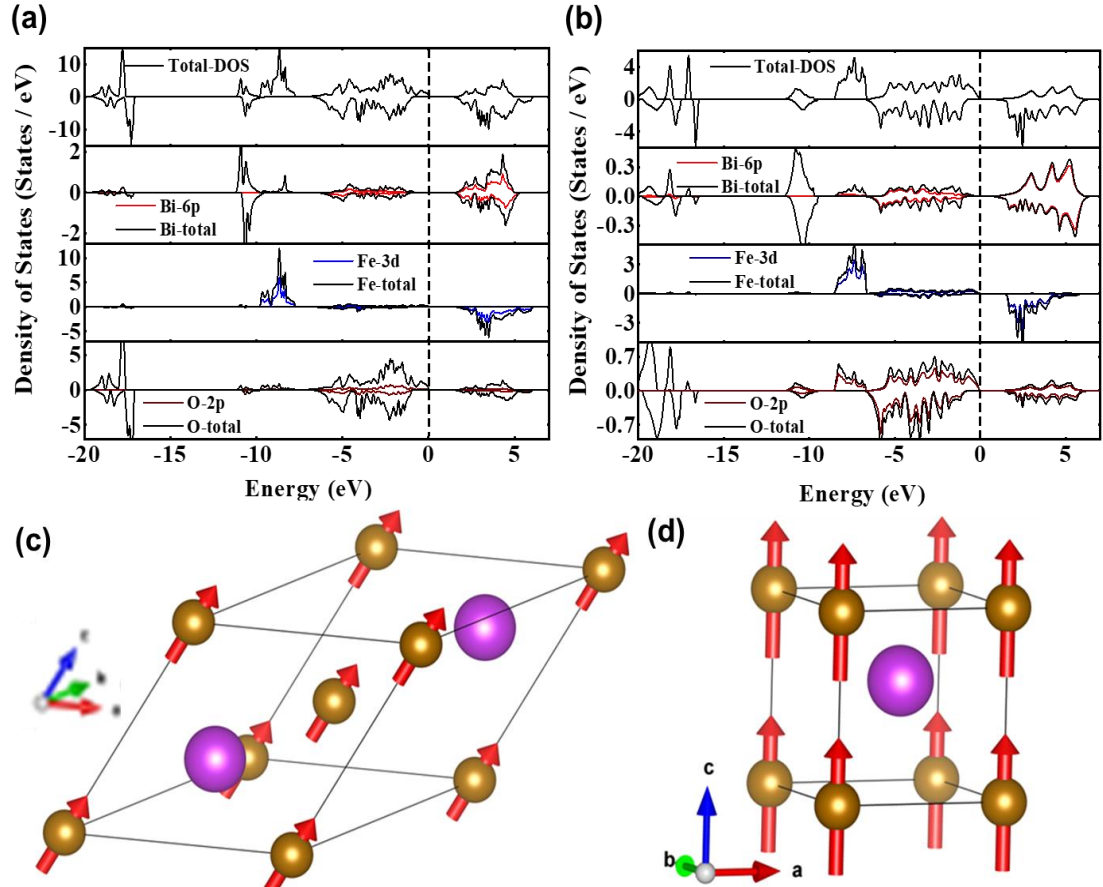


Figure 6: Spin polarised DOS and PDOS of (a) rhombohedral BFO, and (b) triclinic BFO. Ground state magnetic structure of BiFeO₃ derived from DFT calculation (c) Rhombohedral (R3c) and (d) Triclinic (P1).

Hence, the next focus should be on the strain-mediated synthesis of 2D triclinic BFO on a suitable lattice matched substrate and its exploration. The 2D triclinic BFO based heterostructure is expected to demonstrate improved resistivity, high saturation magnetisation, remanence magnetisation and robust magnetoelectric coupling which is essential for the practical implementation of room temperature multiferroic technology.

Conclusions:

The studies on the magnetic properties of the composite BFO/LNMO have been performed, and the combined experimental and theoretical analysis demonstrate the remarkable

improvement of the magnetization and multiferroic magnetoelectric coupling in the composites as compared to the rhombohedral BFO. The enhanced room temperature magnetisation and resistivity in the composites are attributed to the triclinic BFO phase. Interestingly, triclinic BFO has decreased $\langle \text{Fe} - \text{O} - \text{Fe} \rangle$ bond angle and an increased spin canting those results in the significantly increased resistivity and enhanced magnetisation, respectively, as compared to the regular BFO (R3c) structure. Overall, this study introduces triclinic BFO (P1) phase as a promising pathway to realize room temperature multiferroic material and opens a new avenue to overcome the limiting factors of the current multiferroic technology.

Acknowledgements:

Md S. Sheikh and T. K. Bhowmik would like to thank the Department of Science and Technology (DST), Government of India for providing the INSPIRE Fellowship (Sanction No: IF150220 and IF160418, respectively). SS would like to acknowledge CSIR, India for Senior Research Associateship (Scientists' Pool Scheme) in the acknowledgements section.

References

- [1] W.-R. Geng, Y.-L. Tang, Y.-L. Zhu, Y.-J. Wang, B. Wu, L.-X. Yang, Y.-P. Feng, M.-J. Zou, T.-T. Shi, Y. Cao, X.-L. Ma, Magneto–Electric–Optical Coupling in Multiferroic BiFeO₃-Based Films, *Adv. Mater.* **34**, 2106396 (2022).
- [2] Y. L. Huang, D. Nikonov, C. Addiego, R. V. Chopdekar, B. Prasad, L. Zhang, J. Chatterjee, H. J. Liu, A. Farhan, Y. H. Chu, M. Yang, M. Ramesh, Z. Q. Qiu, B. D. Huey, C. C. Lin, T. Gosavi, J. Iniguez, J. Bokor, X. Pan, I. Young, L. W. Martin, and R. Ramesh, Manipulating magnetoelectric energy landscape in multiferroics, *Nat. Commun.* **11**, 2836 (2020).
- [3] D. Sando, A. Barthelemy, and M. Bibes, BiFeO₃ epitaxial thin films and devices: past, present and future, *J. Phys.: Condens. Matter* **26**, 473201 (2014).
- [4] G. Catalan, and J. F. Scott, Physics and applications of bismuth ferrite, *Adv. Mater.* **21**, 2463 (2009).
- [5] D. Yi, P. Yu, Y. C. Chen, H. H. Lee, Q. He, Y. H. Chu, and R. Ramesh, Tailoring Magnetoelectric Coupling in BiFeO₃/La_{0.7}Sr_{0.3}MnO₃ Heterostructure through the Interface Engineering, *Adv. Mater.* **31**, 1806335 (2019).

- [6] J. H. Lee, H. J. Choi, D. Lee, M. G. Kim, C. W. Bark, S. Ryu, M.-A. Oak, and H. M. Jang, Variations of ferroelectric off-centering distortion and 3d-4p orbital mixing in La-doped BiFeO₃ multiferroics, *Phys. Rev. B* **82**, 045113 (2010).
- [7] L. Yin, and W. Mi, Progress in BiFeO₃-based heterostructures: materials, properties and applications, *Nanoscale* **12**, 477 (2020).
- [8] J. Silva, A. Reyes, H. Esparza, H. Camacho, and L. Fuentes, BiFeO₃: A Review on Synthesis, Doping and Crystal Structure, *Integr. Ferroelectr.* **126**, 47 (2011).
- [9] S. Manipatruni, D. E. Nikonov, C. C. Lin, T. A. Gosavi, H. Liu, B. Prasad, Y.-L. Huang, E. Bonturim, R. Ramesh, and I. A. Young, Scalable energy-efficient magnetoelectric spin-orbit logic, *Nature* **565**, 35 (2019).
- [10] A. Haykal, J. Fischer, W. Akhtar, J. Y. Chauleau, D. Sando, A. Finco, F. Godel, Y. A. Birkholzer, C. Carretero, N. Jaouen, M. Bibes, M. Viret, S. Fusil, V. Jacques, and V. Garcia, Antiferromagnetic textures in BiFeO₃ controlled by strain and electric field, *Nat. Commun.* **11**, 1704 (2020).
- [11] N. A. Spaldin, and R. Ramesh, Advances in magnetoelectric multiferroics. *Nat. Mater.* **18**, 203 (2019).
- [12] C. R. Joshi, M. Acharya, G. J. Mankey, and A. Gupta, Effect of thickness and frequency of applied field on the switching dynamics of multiferroic bismuth ferrite thin films, *Phys. Rev. Mater.* **6**, 054409 (2022).
- [13] L. Yin, X. Wang, and W. Mi, Tunable Valley and Spin Polarizations in BiXO₃/BiIrO₃ (X = Fe, Mn) Ferroelectric Superlattices, *ACS Appl. Mater. Interfaces* **10**, 3822 (2018).
- [14] R. Zhang, P. Hu, L. Bai, X. Xie, H. Dong, M. Wen, Z. Mu, X. Zhanga and F. Wu, New multiferroic BiFeO₃ with large polarization, *Phys. Chem. Chem. Phys.* **24**, 5939 (2022).
- [15] S. Saha, R. P. Singh, Y. Liu, A. B. Swain, A. Kumar, V. Subramanian, A. Arockiarajan, G. Srinivasan, and R. Ranjan, Strain transfer in ferroelectric-ferrimagnetic magnetoelectric composite, *Phys. Rev. B* **103**, L140106 (2021).
- [16] N. Wang, X. Luo, L. Han, Z. Zhang, R. Zhang, H. Olin and Y. Yang, Structure, Performance, and Application of BiFeO₃ Nanomaterials, *Nano-Micro Lett.* **12**, 81 (2020).
- [17] R. I. Dass, J.Q. Yan, and J.B. Goodenough, Oxygen stoichiometry, ferromagnetism, and transport properties of La_{2-x}NiMnO_{6+δ}, *Phys. Rev. B* **68**, 064415 (2003).
- [18] M. S. Sheikh, D. Ghosh, A. Dutta, S. Bhattacharyya, and T. P. Sinha, Lead free double perovskite oxides Ln₂NiMnO₆ (Ln = La, Eu, Dy, Lu), a new promising material for photovoltaic application, *Mater. Sci. Eng.: B* **226**, 10 (2017).

- [19] M. S. Sheikh, D. Ghosh, T. K. Bhowmik, A. Dutta, S. Bhattacharyya, and T. P. Sinha, When multiferroics become photoelectrochemical catalysts: A case study with $\text{BiFeO}_3/\text{La}_2\text{NiMnO}_6$, *Mater. Chem. Phys.* **244**, 122685 (2020).
- [20] Z. Chen, S. Prosandeev, Z. L. Luo, W. Ren, Y. Qi, C. W. Huang, L. You, C. Gao, I. A. Kornev, T. Wu, J. Wang, P. Yang, T. Sritharan, L. Bellaiche, and L. Chen, Coexistence of ferroelectric triclinic phases in highly strained BiFeO_3 films, *Phys. Rev. B* **84**, 094116 (2011).
- [21] M. R. Walden, C. V. Ciobanu, and G. L. Brennecke, Density-functional theory calculation of magnetic properties of BiFeO_3 and BiCrO_3 under epitaxial strain, *J. Appl. Phys.* **130**, 104102 (2021).
- [22] B. Xu, S. Meyer, M. J. Verstraete, L. Bellaiche, and B. Dupé, First-principles study of spin spirals in the multiferroic BiFeO_3 *Phys. Rev. B* **103**, 214423 (2021).
- [23] F. Sun, D. Chen, X. Gao, and J.-M. Liu, Emergent strain engineering of multiferroic BiFeO_3 thin films, *J. Materiomics*. **7**, 281 (2021).
- [24] K. Funke, Jump relaxation in solid electrolytes, *Prog. Solid State Chem.* **22**, 111 (1993).
- [25] A. K. Jonscher, *Dielectric Relaxation in Solids*, Chelsea Dielectrics Press, London, 1983.
- [26] E. F. Hairetdinov, N. F. Uvarov, H. K. Patel, and S. W. Martin, Estimation of the free-charge carrier concentration in fast-ion conducting $\text{Na}_2\text{S-B}_2\text{S}_3$ glasses from an analysis of the frequency-dependent conductivity, *Phys. Rev. B* **50**, 13259 (1994).
- [27] M. S. Sheikh, A. P. Sakhya, A. Dutta, and T. P. Sinha, Light induced charge transport in $\text{La}_2\text{NiMnO}_6$ based Schottky diode, *J. Alloys Compd.* **727**, 238 (2017).
- [28] N. S. Rogado, J. Li, A. W. Sleight, and M. A. Subramanian, Magnetocapacitance and Magnetoresistance Near Room Temperature in a Ferromagnetic Semiconductor: $\text{La}_2\text{NiMnO}_6$, *Adv. Mater.* **17**, 2225 (2005).
- [29] S. Zhao, L. Shia, S. Zhou, J. Zhao, H. Yang, and Y. Guo, Size-dependent magnetic properties and Raman spectra of $\text{La}_2\text{NiMnO}_6$ nanoparticles, *J. Appl. Phys.* **106**, 123901 (2009).
- [30] N. Gao, C. Quan, Y. Ma, Y. Han, Z. Wu, W. Mao, J. Zhang, J. Yang, X. Li, W. Huang, Experimental and first principles investigation of the multiferroics BiFeO_3 and $\text{Bi}_{0.9}\text{Ca}_{0.1}\text{FeO}_3$: Structure, electronic, optical and magnetic properties, *Physica B: Condens. Mat.* **481**, 45 (2016).
- [31] C. Ederer, and N. A. Spaldin, Weak ferromagnetism and magnetoelectric coupling in bismuth ferrite, *Phys. Rev. B* **71**, 060401(R) (2005).
- [32] M. Rangi, A. Agarwal, S. Sanghi, R. Singh, S.S. Meena, and A. Das, Crystal structure and magnetic properties of $\text{Bi}_{0.8}\text{A}_{0.2}\text{FeO}_3$ (A = La, Ca, Sr, Ba) multiferroics using neutron diffraction and Mossbauer spectroscopy, *AIP. Adv.* **4**, 87121 (2014).

- [33] G. L. Yuan, Siu Wing, J. M. Liu, and Z. G. Liu, Structural transformation and ferroelectromagnetic behavior in single-phase $\text{Bi}_{1-x}\text{Nd}_x\text{FeO}_3$ multiferroic ceramics, *Appl. Phys. Lett.* **89**, 052905 (2006).
- [34] I. Sosnowska, T. P. Neumaier, and E. Steichele, Spiral magnetic ordering in bismuth ferrite, *J. Phys. C: Solid State Phys.* **15**, 4835 (1982).
- [35] P. Hermet, M. Goffinet, J. Kreisel, and Ph. Ghosez, Raman and infrared spectra of multiferroic bismuth ferrite from first principles, *Phys. Rev. B* **75**, 220102(R) (2007),
- [36] T. K. Bhowmik, and T. P. Sinha, Phase driven magnetic and optoelectronic properties of $\text{La}_2\text{CrNiO}_6$: A DFT and Monte Carlo perspective, *J. Solid State Chem.* **304**, 122570 (2021).

Triclinic BiFeO₃: A new magnetic phase with enhanced magnetism and resistivity

Md Sariful Sheikh ^{a, 1, †, *}, Tushar K. Bhowmik ^{a, †, *}, Alo Dutta ^b, Sujoy Saha ^c, Chhatra R. Joshi ^d, T. P. Sinha ^a

^a Department of Physics, Bose Institute, 93/1, A.P. C. Road, Kolkata-700009, India

^b Department of Condensed Matter Physics and Material Sciences, S.N. Bose National Centre for Basic Sciences, Block-JD, Sector-III, Salt Lake, Kolkata, 700106, India

^c Department of Materials Engineering, Indian Institute of Science, Bangalore 560012, India

^d Department of Physics and Astronomy, The University of Alabama, Tuscaloosa, AL 35487, USA

1. (1-x)BFO + (x)LNMO (X = 0.0, 0.1, 0.2, 0.3) pellet formation

The sol-gel synthesis of the multiferroic composite (1-x)(BFO) + x(LNMO) (with x = 0.0, 0.1, 0.2 and 0.3) powders are reported in our previous work [1]. First, the reagent grade metal nitrates, Bi(NO₃)₃.5H₂O, Fe(NO₃)₃.6H₂O, La(NO₃)₃.3H₂O, Ni(NO₃)₂.4H₂O and Mn(NO₃)₂.6H₂O are dissolved in 2-methoxy ethanol solvent. 3% of extra Bi(NO₃)₃.5H₂O was taken to avoid the Bi evaporation loss during heating process. A solution of tartaric acid in 2-methoxy ethanol (in 1:1 molar ratio with the metal nitrates) is added drop wise in the first solution and mixed well. The well mixed solutions were dried at 393 K to get the black precursor powder. Finally, the precursor powders are heated in ambient furnace in two steps heating method. In the first step, the samples are heated at 723 K for 2 hours to ensure the complete phase formation of BFO. In the second step, the furnace temperature is gradually increased to 923 K from 723 K and heated for 5 hours to ensure the complete double perovskite phase formation of LNMO. Finally, the furnace is cooled down to the room temperature at a cooling rate of 1 K/min. The synthesised powders are palletised into circular discs of average diameter 100 mm and thickness 2 mm using polyvinyl alcohol as the binder and sintered at 973 K for 3 hours for the magnetic and dielectric measurements.

¹ Present address: Department of Materials Science and Engineering, University of Wisconsin Madison, 1509 University Ave, Madison, WI 53706, United States

[†] Authors contributed equally to this work.

Supporting information file

Table S1: Lattice parameters of the BiFeO_3 and $\text{La}_2\text{NiMnO}_6$ phases in the $(1-x)\text{BiFeO}_3 + (x)\text{La}_2\text{NiMnO}_6$ composites

Lattice parameters	$x = 0.0$	$x = 0.1$		$x = 0.2$		$x = 0.3$	
	BFO (R3c)	BFO (P1)	LNMO ($\text{P2}_1/\text{n}$)	BFO (P1)	LNMO ($\text{P2}_1/\text{n}$)	BFO (P1)	LNMO ($\text{P2}_1/\text{n}$)
a (\AA)	5.643	3.931	5.572	3.907	5.543	3.881	5.530
b (\AA)	5.643	3.936	5.588	3.952	5.567	3.939	5.554
c (\AA)	5.643	3.956	7.821	3.928	7.777	3.914	7.772

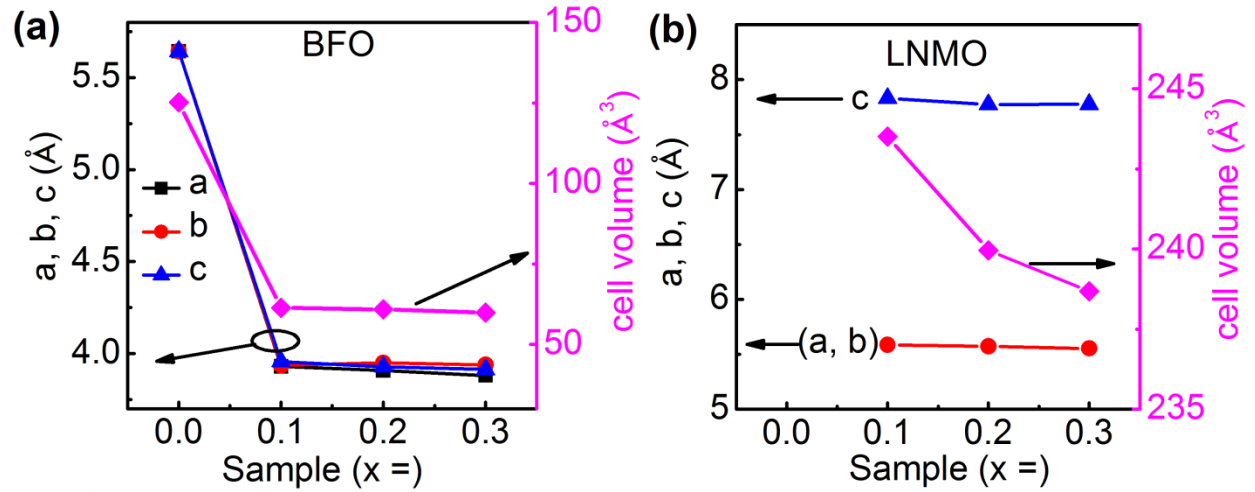


Figure S1. Lattice parameters of (a) BFO and (b) LNMO in the composites.

Supporting information file

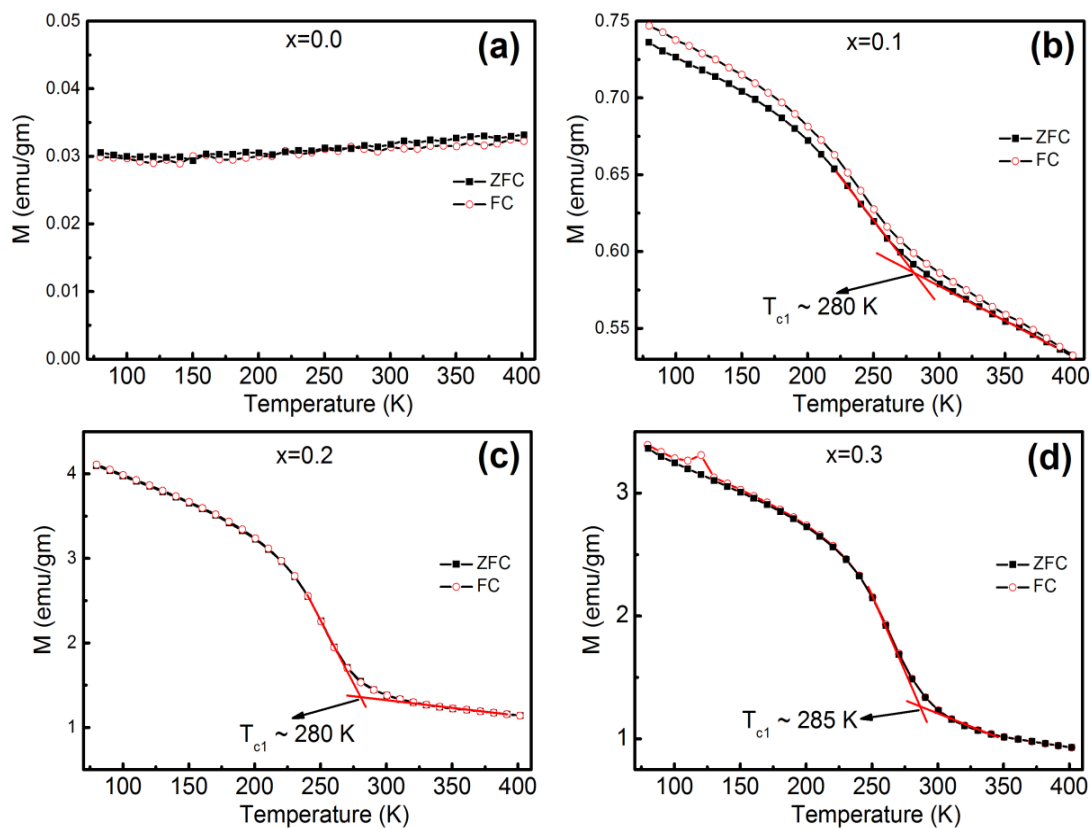


Figure S2. Temperature dependent magnetisation of sample (a) $x=0.0$, (b) $x=0.1$, (c) $x=0.2$ and (d) $x=0.3$. T_{c1} represents the ferromagnetic Curie temperature of the LNMO phase.

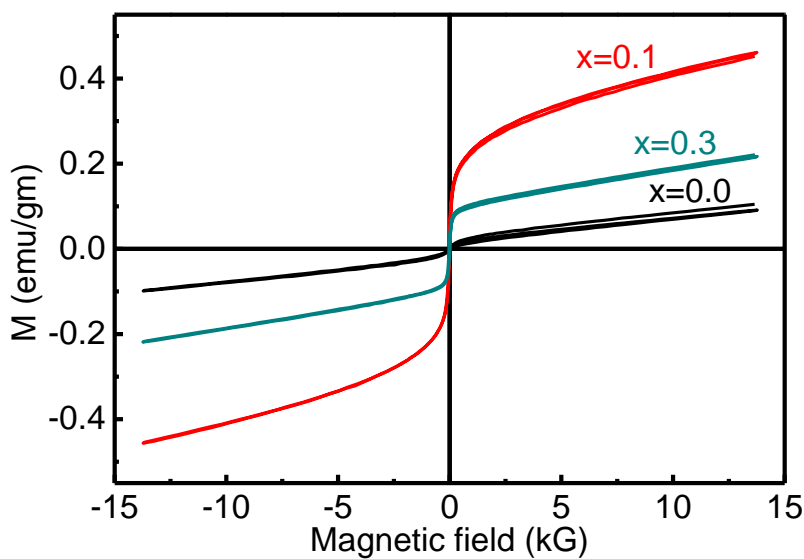


Figure S3: MH loop at 803 K.

Supporting information file

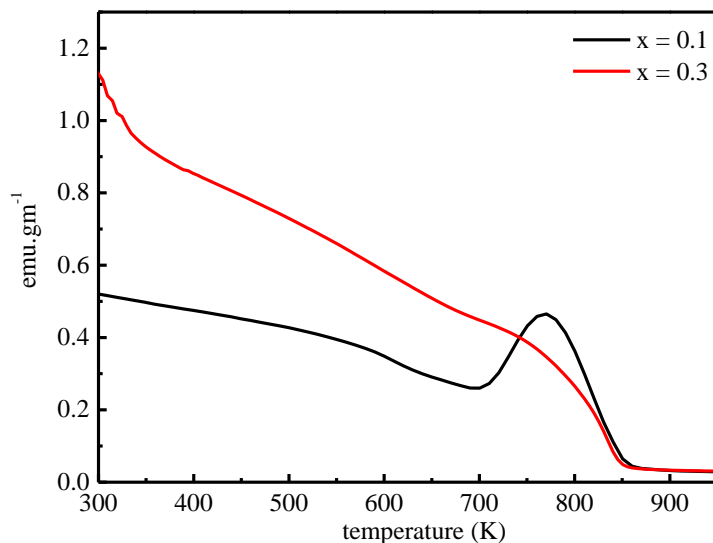


Figure S4: High temperature magnetisation curve collected during zero field cooling at a magnetic field of 5kOe of samples with $x=0.1$ and 0.3 .

Table S2: Magnetic parameters derived from the M-H hysteresis loop at 300 K.

Sample	M_r (emu/gm)	M_s (emu/gm)	H_{cr} (emu/gm)
$x = 0.0$	0.0003	0.088	0.035
$x = 0.1$	0.304	0.922	0.188
$x = 0.2$	0.425	1.551	0.195
$x = 0.3$	0.332	1.498	0.149

Table S3: Magnetic parameters derived from the M-H hysteresis loop at 80 K.

Sample	M_r	M_s	H_{cr}
$x = 0.0$	0.0005	0.087	0.051
$x = 0.1$	0.383	1.149	0.252
$x = 0.2$	1.076	5.17	0.347
$x = 0.3$	0.766	4.822	0.302

Supporting information file

Table S4: Comparison of the magnetic moment of sample with $x = 0.2$ with some recent bulk BFO based magnetic materials.

Material	M_r (emu/gm)	Year	temperature
0.8BFO + 0.2LNMO	0.425	This work	300 K
0.7BFO + 0.3TbMnO ₃ ^[2]	~ 0.15	2019	275 K
Bi _{0.95} Gd _{0.05} FeO ₃ ^[3]	0.218	2019	RT
Bi _{1-x} Ca _x FeO ₃ ($x=0.1$) ^[4]	0.096	2019	RT
0.8(Bi _{0.9} La _{0.1} FeO ₃)–0.2(KBr) ^[5]	~ 0.25	2019	300 K
BiFe _{1-x} Se _x O ₃ $x=0.25$ ^[6]	0.034	2019	300 K
Bi _{0.92} La _{0.08} Fe _{1-x} Se _x O ₃ $x=0$ ^[6]	0.1334	2019	300 K
Bi _{0.5} La _{0.5} Fe _{0.5} Mn _{0.5} O ₃ ^[7]	0.7 emu/g (Much lower at RT)	2017	2 K

2. Model and Monte-Carlo Simulation:

The temperature dependent magnetic properties of BFO/LNMO composite are analysed through the Monte-Carlo simulation method. For the triclinic BFO structure, we have considered the only one magnetic ion Fe³⁺ ion at corner edges [8]. Now, we have considered the anisotropic 3D-Ising model for the simulation whereas any other models like Heisenberg model does not satisfy the experimental data so accurately. So, the Ising model Hamiltonian with nearest- neighbour (nn) and next nearest- neighbour (nnn) interactions are described as

Supporting information file

$$H = -J_1 \sum_{\langle i,j \rangle} S_i S_j - J_2 \sum_{\langle\langle i,k \rangle\rangle} S_i S_k - \Delta \sum_k S_k^2 - h \sum_i S_i,$$

Where S_i , S_j and S_k are the spins at lattice sites i , j and k respectively. $\sum_{\langle i,j \rangle}$ and $\sum_{\langle\langle i,k \rangle\rangle}$ are the summations made over spin pairs coupled through the nn interaction constant J_{ij} and nnn interaction constant J_{ik} respectively, the magnetocrystalline anisotropy energy constant (Δ) -24.8 $\mu\text{eV/Fe}$ is taken from previous study [9] and h is the external magnetic field applied along z- axis. For the complex perovskite $[(1-x)(\text{BFO}) + x(\text{LNMO})_x]$ ($x = 0.1, 0.2, 0.3$), we have taken two sublattices; one is for BiFeO_3 and another for $\text{La}_2\text{NiMnO}_6$. The whole complex perovskite consists of the three magnetic ions, Fe^{3+} , Ni^{2+} and Mn^{4+} . So, there are six spin spin interactions present in the system and the interaction constants are $J_{\text{Fe-Fe}}$, $J_{\text{Ni-Ni}}$, $J_{\text{Mn-Mn}}$, $J_{\text{Ni-Mn}}$, $J_{\text{Fe-Ni}}$, and $J_{\text{Fe-Mn}}$. But, the interaction between Fe-Ni and Fe-Mn are very small due to the small concentration of LNMO and large atomic distance between these atoms. So, the nearest neighbour interactions are $J_{I(\text{Fe-Fe})}$, $J_{I(\text{Ni-Mn})}$, $J_{I(\text{Ni-Ni})}$, and $J_{I(\text{Mn-Mn})}$. The next nearest neighbours are $J_{2(\text{Fe-Fe})}$, $J_{2(\text{Ni-Mn})}$, $J_{2(\text{Ni-Ni})}$, and $J_{2(\text{Mn-Mn})}$. BFO has antiferromagnetic ordering temperature (T_N) around 630 K [10]. The nn ($J_{I(\text{Fe-Fe})}$) and nnn ($J_{2(\text{Fe-Fe})}$) interactions in BFO sublattice are antiferromagnetic and weakly ferromagnetic respectively. The $\text{La}_2\text{NiMnO}_6$ has a paramagnetic to ferromagnetic transition around 280 K upon cooling. So, the interactions between Ni-Ni, Mn-Mn, and Ni-Mn are ferromagnetic. Masrour et. al. has determined the interaction constants for LNMO from the mean-field theoretical calculations. The values are $J_{I(\text{Ni-Mn})} = 15.0$ K, $J_{I(\text{Ni-Ni})} = 22.0$ K, $J_{I(\text{Mn-Mn})} = 24.0$ K, $J_{2(\text{Ni-Mn})} = 10.0$ K, $J_{2(\text{Ni-Ni})} = 19.0$ K, and $J_{2(\text{Mn-Mn})} = 23.0$ K. We have taken the spin magnitude of Fe^{3+} , Ni^{3+} and Mn^{3+} are 5/2, 3/2 and 2 respectively. For BFO sublattice we have determined the interaction constants from the mean field approximation. The formula is given by

$$T_N = \frac{2}{3K_B} ZS(S+1)J_{\text{Fe-Fe}},$$

Supporting information file

Where Z is the coordination number and S is the spin value of all Fe^{3+} ions. T_N denotes the experimental value of the transition temperature (630 K) and $J_{\text{Fe-Fe}}$ is the interaction constant and K_B is Boltzmann constant. The calculated value of $J_{\text{Fe-Fe}}$ turns out to be 18.0 K. Now the strong AFM interaction between nearest neighbours is significantly high over the weak FM interaction between next nearest neighbours. So, we have neglected the nnn interaction constant $J_{2(\text{Fe-Fe})}$. The $J_{I(\text{Fe-Fe})}$ is now equivalent to $J_{(\text{Fe-Fe})}$.

The magnetic properties of the BFO and BFO/LNMO composites are analysed using Monte Carlo simulation (MCS) under the Metropolis algorithm using the above-described Hamiltonian with cyclic boundary conditions on the lattice [11, 12]. We have performed this MCS on the sample of dimension $N = L \times L \times L$, where L is the number of unit cells in all three directions. We have taken $N = 32 \times 32 \times 32$ number of lattices for these simulations. The single-spin flip mechanism is used for all lattice sites to minimize the internal energy and the flips of these spin values are accepted or rejected according to the Boltzmann statistics [12]. At each temperature for every spin configuration, a number of 10^5 Monte Carlo steps have been performed to equilibrating the lattice and next 10^6 steps for thermal average of the total magnetisation, $M = \frac{1}{N} \langle \sum_i s_i \rangle$. Where the sum is performed over all spin values of Fe^{3+} , Ni^{3+} and Mn^{3+} and $\langle \dots \rangle$ indicates the statistical time average.

3. DFT Calculation method:

The electronic structure of BiFeO_3 has been investigated using the full potential linearized augmented plane wave as implemented in the WIEN2K code. The generalised gradient approximation (GGA) with the Hubbard parameter (U) method has been taken to study the spin polarised electronic band structure calculations. The experimental structure is optimized through

Supporting information file

the energy minimization. After that, the optimized lattice parameters are used for further calculations. The minimization energy for R3c structure is -92320.459316 Ry, whereas the triclinic BFO has shown -46159.01110835 Ry for the optimized structure. The **Table S5** shows the lattice parameters before and after energy minimization, suggesting the stability of the structures. The threshold energy between valence and core states is fixed to -7 Ry for both triclinic and rhombohedral structures. The maximum angular momentum, l_{\max} for the wave function expansion inside the atomic spheres is set at 10 and the plane wave cut off $R_{\text{MT}} \times K_{\text{Max}}$ is taken to 7 Ry with 1000 k points mesh integration over the first Brillouin zone to solve the Kohn- Sham equations. Here, the R_{MT} and K_{Max} stand for the average Muffin-Tin radii of the ionic sphere and the wave function cut-off. The Muffin-Tin radii of BFO under triclinic P1 space group are 2.16 Å, 1.69 Å and 1.46 Å for Bi, Fe and O atoms respectively whereas for rhombohedral R3c they are 2.5 Å, 1.9 Å and 1.63 Å. The energy and charge cut-off are set to 10^{-4} Ry and 10^{-3} e for the self-consistent convergence in the scf cycles. The effective U value for the strong correlation between Fe-3d orbital electrons is set to 6 eV for both the cases.

Table S5: Lattice parameter used for the DFT calculations (before and after energy minimization)

Symmetry		a (Å)	b (Å)	c (Å)	α	β	γ
BFO (R3c)	Before	5.58720	5.58720	13.89070	90	90	120
	After	5.52165	5.52165	13.72870	90	90	120
BFO (P1)	Before	3.93100	3.93100	3.93100	90.32	90.24	89.98
	After	3.93104	3.93104	3.93104	90.3194	90.2443	89.9762

Supporting information file

4. References:

- [1] Md S. Sheikh, D. Ghosh, T. K. Bhowmik, A. Dutta, S. Bhattacharyya, TP Sinha, When multiferroics become photoelectrochemical catalysts: A case study with $\text{BiFeO}_3/\text{La}_2\text{NiMnO}_6$, *Materials Chemistry and Physics* 244, 2020, 122685.
- [2] Gupta et al., Room temperature exchange bias in antiferromagnetic composite $\text{BiFeO}_3\text{-TbMnO}_3$, *J. Appl. Phys.* 126, 243903 (2019).
- [3] M. A. Matin, M. N. Hossain, M. A. Hakim, M. F. Islam, Effects of Gd and Cr co-doping on structural and magnetic properties of BiFeO_3 nanoparticles, 2019 *Mater. Res. Express* 6, 055038.
- [4] Huimin Xian, Lingyun Tang, Zhongquan Mao, Jiang Zhang, Xi Chen, Bounded Magnetic Polarons Induced Enhanced Magnetism in Ca-doped BiFeO_3 , *Solid State Communications* (2018), doi: 10.1016/j.ssc.2018.09.009.
- [5] Karpinsky, et al., Ferromagnetic-like behavior of $\text{Bi}_{0.9}\text{La}_{0.1}\text{FeO}_3\text{-KBr}$ nanocomposites, *Scientific Reports* (2019) 9:10417.
- [6] Syed Rizwan, Muhammad Umar, Zaheer Ud Din Babar, Saif Ullah Awan, and M. Anis ur Rehman, Selenium-enriched flower-like of bismuth ferrite nanosheets assembly with associated magnetic properties, *AIP Advances* 9, 055025 (2019).
- [7] R. Singh, P. K. Gupta, S. Kumar, A. G. Joshi, A. K. Ghosh, S. Patil, and S. Chatterjee, Enhancement in electrical and magnetic properties with Ti-doping in $\text{Bi}_{0.5}\text{La}_{0.5}\text{Fe}_{0.5}\text{Mn}_{0.5}\text{O}_3$, *Journal of Applied Physics* 121, 154101 (2017).
- [8] Samia Yahyaoui, Sami Kallel, H.T. Diep, Magnetic properties of perovskites $\text{La}_{0.7}\text{Sr}_{0.3}\text{Mn}^{3+}_{0.7}\text{Mn}^{4+}_{0.3-x}\text{Ti}_x\text{O}_3$: Monte Carlo simulation versus experiments, *Journal of Magnetism and Magnetic Materials* 416 (2016) 441–448.
- [9] J. T. Zhang, X. M. Lu, J. Zhou, H. Sun, J. Su, C. C. Ju, F. Z. Huang, and J. S. Zhu, Origin of magnetic anisotropy and spiral spin order in multiferroic BiFeO_3 , *Appl. Phys. Lett.* 100, 242413 (2012).
- [10] P Fischer, M Polomska, I Sosnowska and M Szymanski, Temperature dependence of the crystal and magnetic structures of BiFeO_3 , *J. Phys. C: Solid St. Phys.*, 13 (1980) 1931-1940.
- [11] David P. Landau, Kurt Binder, *A Guide to Monte Carlo Simulations in Statistical Physics*, Third Edition, Cambridge University Press, New York, 2009.
- [12] M. E. J. Newman, G. T. Barkema, *Monte Carlo Methods in Statistical Physics*, Oxford University Press Inc., New York, 1999